

Functionalizable Nanomorphology Gradients via Colloidal Self-Assembly

Christoph Huwiler,[†] Tobias P. Kunzler,[‡] Marcus Textor,[‡] Janos Vörös,[†] and Nicholas D. Spencer^{*‡}

Laboratory of Biosensors and Bioelectronics, Institute of Biomedical Engineering, Department of Information Technology and Electrical Engineering, ETH Zürich, Gloriastrasse 35, CH-8092 Zurich, Switzerland, and Laboratory for Surface Science and Technology, Department of Materials and Materials Research Center, ETH Zürich, Wolfgang-Pauli-Strasse 10, CH-8093 Zürich, Switzerland

Received January 8, 2007. In Final Form: February 26, 2007

We present a novel approach for the fabrication of tailored nanomorphology gradients on metal oxide surfaces. We first show the direct formation of a nanocolloidal density gradient by a dip-coating process. The obtained silica nanoparticle gradients are then subjected to a heat treatment. Control of this sintering step allows the precise tailoring of the particle morphology on the surface. Both these processes together provide a new tool to form precise, tunable, and material-independent nanomorphology gradients.

Introduction

Surfaces with a continuously changing surface parameter (gradient surfaces) have distinct advantages for certain applications. Such surfaces, for example, allow rapid screening tests or combinatorial diagnostic studies to be performed on a single sample, which is of particular importance in biotechnology or medicine. The surface parameters of interest range from crystallinity¹ to porosity² and surface chemistry. Among surface-chemistry parameters that have been varied along gradients, wettability has been reported most frequently. In these gradients, the wettability changes gradually along the length of the sample because of a controlled change in surface chemistry. Various methods have been developed to produce such wettability gradients.^{3–6}

Another parameter that plays a crucial role, especially in many bioscience applications, is surface morphology. It has been known for a long time that surface roughness affects the biological response to surfaces (e.g., cell adhesion, proliferation, and differentiation). Also, parameters related to surface-contact effects (such as tribological or adhesion phenomena) will be influenced by a varying surface topography. However, only little progress has been made in producing large-scale topographical gradients. Crystallinity gradients of a polymer film induced by a temperature-gradient stage have been described previously,¹ as have gradients of pore size in silicon, fabricated by etching in an anisotropic electric field.² Only very recently, an approach was presented by Kunzler et al. that allows the production of stochastic roughness

gradients over centimeter length-scales with topographical features in the nanometer and micrometer range.⁷

A different approach to the production of surface morphology gradients is to capitalize on the self-assembly potential of colloidal particles. To date, the only particle-gradient structures produced have been colloidal crystals for use as photonic band gap materials. Most of these colloidal crystal gradients are fabricated by means of polymer-infiltration techniques, where a polymer with a gradually changing refractive index is forced into the interstices of a colloidal crystal.^{8,9} It was not until recently that the first colloidal crystal gradients were produced.^{10–12} An indirect way of producing a number-density gradient of colloidal particles was presented by Bhat et al. They decorated a molecular gradient (of amino groups) with colloidal gold particles to obtain nanocolloidal density gradients.¹³ A similar approach was also presented by the same group to produce gold nanoparticle density gradients in two orthogonal directions.¹⁴

In this article, an alternative way of producing a particle-density gradient on a surface using nanosized colloidal particles is presented. In a simple dip-coating process, a gradient in nanoparticle density is achieved directly on the substrate. The number density can be varied from a high-coverage, random monolayer at one end of the gradient to only a few particles per square micrometer on the other. Not only is this method very universal as far as substrate and particle materials are concerned, but we also show how the shape of the colloidal particles on the substrate can be varied over a wide range using a heat-treatment step. This heat-treatment step simultaneously increases the adhesion of the particles to the substrate, providing the necessary robustness for such particle gradients to be used in replication techniques or in experiments that require a robust morphology gradient (e.g., in cell biology experiments).

* To whom correspondence should be addressed. E-mail: spencer@mat.ethz.ch.

[†] Laboratory of Biosensors and Bioelectronics, ETH Zürich.

[‡] Laboratory for Surface Science and Technology, ETH Zürich.

(1) Washburn, N. R.; Yamada, K. M.; Simon, C. G.; Kennedy, S. B.; Amis, E. *Biomaterials* **2004**, *25*, 1215.

(2) Karlsson, L. M.; Tengvall, P.; Lundström, I.; Arwin, H. *J. Electrochem. Soc.* **2002**, *149*, C648.

(3) Elwing, H.; Welin, S.; Askendal, A.; Nilsson, U.; Lundstroem, I. *J. Colloid Interface Sci.* **1987**, *119*, 203.

(4) Lee, J. H.; Kim, H. G.; Khang, G. S.; Lee, H. B.; Jhon, M. S. *J. Colloid Interface Sci.* **1992**, *151*, 563.

(5) Liedberg, B.; Tengvall, P. *Langmuir* **1995**, *11*, 3821.

(6) Morgenthaler, S.; Lee, S.; Zürcher, S.; Spencer, N. D. *Langmuir* **2003**, *19*, 10459.

(7) Kunzler, T. P.; Drobek, T.; Sprecher, C. M.; Schuler, M.; Spencer, N. D. *Appl. Surf. Sci.* **2006**, *253*, 2148.

(8) Park, J.-H.; Choi, W. S.; Koo, H. Y.; Kim, D.-Y. *Adv. Mater.* **2005**, *17*, 879.

(9) von Freymann, G.; John, S.; Kitaev, V.; Ozin, G. A. *Adv. Mater.* **2005**, *17*, 1273.

(10) Abkarian, M.; Nunes, J.; Stone, H. A. *Langmuir* **2004**, *126*, 5978.

(11) Li, J.; Han, Y. *Langmuir* **2006**, *22*, 1885.

(12) Zhang, J.; Xue, L.; Han, Y. *Langmuir* **2005**, *21*, 5667.

(13) Bhat, R. R.; Fischer, D. A.; Genzer, J. *Langmuir* **2002**, *18*, 5640.

(14) Bhat, R. R.; Tomlinson, M. R.; Genzer, J. *Macromol. Rapid Commun.* **2004**, *25*, 270.

Experimental Section

Colloidal Gradient Preparation. Negatively charged silica particles will readily adsorb onto a positively charged surface by electrostatic attraction. To provide such a positively charged surface, a thin film of poly(ethylene imine) (PEI) (a branched, cationic polyelectrolyte polymer,¹⁵ Sigma-Aldrich, Germany) was adsorbed onto a silicon wafer surface, previously cleaned by ultrasonication (10 min in isopropanol and then in Millipore water for another 10 min). The samples were then oxygen plasma treated at radio frequency (RF) level “Hi” (PDC-002, Harrick Plasma, Ithaca, United States) for 3 min. Cleaned samples were immersed in 1 mg/mL filtered PEI solution in ultrapure water for 30 min. After adsorption of the PEI electrolyte, the silicon wafer pieces were rinsed with ultrapure water, were blown dry in a nitrogen jet, and were stored in a closed container at room temperature. Measurements of PEI-coated particles exhibited a positive ζ -potential of around 30 mV at neutral pH, indicating that a PEI-coated surface is indeed positively charged at neutral pH values.

The nanoparticle gradients were produced using a suspension with silica particles with an average diameter of 73 nm (Klebosol, Clariant, France). The particle diameter was determined using scanning electron microscopy (SEM) and X-ray disc centrifuge methods. ζ -Potential experiments were conducted over a large pH range, and the surface charge (ζ -potential) was -60 mV at a pH of 7. The original, unfiltered 30 wt % stock suspension was homogenized for 5 min in an ultrasonic bath and was diluted to 1 wt % with ultrapure water, HEPES 1 (10 mM 4-(2-hydroxyethyl)piperazine-1-ethane-sulfonic acid, adjusted to pH 7.4 with 6 M NaOH) or HEPES 2 (HEPES 1 with 150 mM NaCl). This 1 wt % suspension was further diluted with ultrapure water, HEPES 1 or HEPES 2, to a final 0.002 wt % working suspension. Before use, the working suspension was homogenized again for 5 min in an ultrasonic bath. No ion exchange was performed prior to experiments.

The PEI-coated substrate was lowered into the colloidal suspension with a linear-motion drive (Owis Staufen, Germany). The immersion profile was set to $x(t) = a(t - u)^2$, where $x(t)$ is the position on the gradient at time t , which was running from 0 to 1800 s, $u = -100$ s (a parameter needed only for technical reasons), and $a = -3 \times 10^{-6}$ m/s². This setup results in the creation of a gradient over 10 mm after a total immersion time of 30 min. The suspension was kept slightly agitated during the procedure. Upon completion of the immersion process, the beaker containing the suspension was immediately flushed with about 1000 mL of distilled water to remove the particle suspension and to prevent further particles adsorbing onto the substrate. Afterward, the substrate was rinsed with ultrapure water and was blown dry with a nitrogen jet.

Sintering of Colloidal Gradients. Sintering of the gradient substrates was carried out in a high-temperature furnace under ambient atmosphere. Substrates were heated at 10 °C/min to final temperatures of either 1075, 1100, 1125, 1150, 1175, or 1200 °C, were held for 2 h, and then were cooled down at 1.5 °C/min to room temperature. To determine the “contact angles” shown in Figure 7, SEM images were analyzed using image analysis software (image J). The sintered gradient samples were tilted in the SEM to allow for a side view of the surface and to achieve a more reliable estimation of the contact angle.

Cell Culture. To achieve a more cell-compatible surface environment, the entire particle gradient was dipped into a PLL-g-PEG-RGD solution. The RGD-peptide sequence is end-grafted to the PLL-g-PEG copolymer and is known to promote cell attachment by interacting with cell integrins.^{16,17} Rat calvarial osteoblasts (RCO) were cultivated for 7 days on a particle gradient with the following seeding conditions: 6000 cells/cm² in α -DMEM with 10% fetal bovine serum and 1% antibiotics medium, incubation at 37 °C, 7% CO₂, 100% humidity. After 7 days of culture, the cells were fixed,

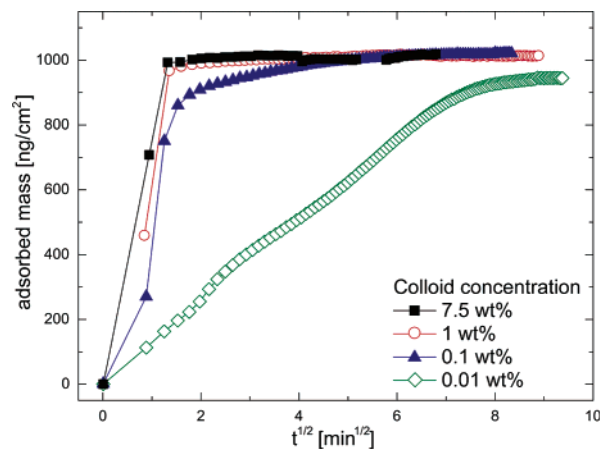


Figure 1. Influence of colloid concentration on the adsorption behavior of 73 nm silica colloids buffered in HEPES 1 (10 mmol salt concentration) at pH 7.4 on a poly(ethylene imine) coated silicon wafer observed by OWLS (optical waveguide light-mode spectroscopy). The negatively charged silica nano colloids adsorb electrostatically onto the positively charged PEI coated surface. OWLS is a surface-sensitive optical detection technique used to monitor adsorption processes in situ.

and the nucleus was stained with DAPI and the actin network with phalloidin as described by Kunzler et al.¹⁸

Results and Discussion

Silica particles, 73 nm in diameter, adsorb onto a PEI-coated silica surface in a controllable way, as shown in Figure 1. Depending on the concentration of the colloidal particles in the suspension, a monolayer of particles adsorbs onto the PEI-coated silica surface very rapidly, over a time span of several minutes. With a particle concentration of more than 1 wt %, adsorption of a monolayer takes place in less than a minute. For dilute suspensions, say 0.01 wt %, adsorption requires in excess of 1 h to produce a complete monolayer. The extent of this adsorption process is proportional to \sqrt{t} , as discussed later in this section.

The adsorption of colloidal particles by electrostatic interactions may be viewed as a one-step process, where a particle adsorbs electrostatically onto the substrate and may no longer be moved on the surface. Such processes are often referred to as irreversible “random sequential adsorption” (RSA),^{19,20} where particles “stick” to a surface and cannot be moved after adsorption. As a consequence, a jamming limit exists for the particle coverage, which is found to be 0.547.²¹ This means that the theoretical maximum surface coverage for the system used in this work may not exceed 54.7%. However, this value may, in reality, not be reached, since the particles are not only defined by their “physical” size, but also by the electric double layer around them. This double layer has a finite thickness, which must be added to the particle’s physical diameter. Thus, the longer ranging the electric double layer, the lower the particle surface coverage at the jamming limit. The thickness and the numeric value of the electric double layer can readily be influenced by pH and ionic strength. In Figure 2, a schematic representation of the RSA model is given and corresponding SEM images are shown to illustrate the situation in our real system. At the jamming limit (Figure 2b), no more particles (or disks) may be deposited without moving particles on the surface (some of the forbidden particle positions

(15) Pericet-Camara, R.; Papastavrou, G.; Behrens, S. H.; Helm, C. A.; Bokovec, M. *J. Colloid Interface Sci.* **2006**, *296*, 496.

(16) Ruoslahti, E. *Annu. Rev. Cell Dev. Biol.* **1996**, *12*, 697.

(17) Schuler, M.; Owen, G. R.; Hamilton, D. W.; De Wild, M.; Textor, M.; Brunette, D. M.; Tosatti, S. *Biomaterials* **2006**, *27*, 4003.

(18) Kunzler, T. P.; Drobek, T.; Schuler, M.; Spencer, N. D. *Biomaterials* **2007**, *28*, 2175.

(19) Evans, J. W. *Rev. Mod. Phys.* **1993**, *65*, 1281.

(20) Hinrichsen, E. L.; Feder, J.; Jossang, T. *J. Stat. Phys.* **1986**, *44*, 793.

(21) Feder, J. *J. Theor. Biol.* **1980**, *87*, 237.

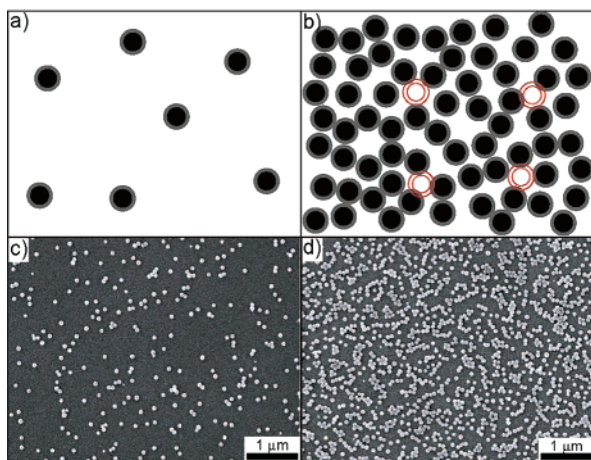


Figure 2. Random sequential adsorption model sketch and SEM images illustrating two stages of the process. (a) After short times (and depending on particle concentration), a few particles have irreversibly adsorbed to the surface. They cannot be moved on the surface, since they are strongly bound by electrostatic forces. (b) At or near the jamming limit of the RSA model: no further particles can be deposited, since they would overlap (some of the forbidden positions are indicated with red, hollow spheres). The effective “radius” of the particle consists not only of the particle itself but also of the ion cloud that it carries (symbolized by the gray ring around each black particle). This electric double layer (characterized by the Debye length) can be changed by varying pH or ionic strength of the solution. Increasing the Debye length therefore lowers the actual particle density on the surface. (c, d) SEM images of 73 nm silica particles adsorbing on a positively charged PEI surface. (c) After short times, a few particles have adsorbed on the surface. At this stage, some deviation of the RSA model can be observed, such as clustering of a few particles. (d) After longer adsorption times (30 min), a complete RSA “monolayer” forms as shown in b. Also in this image, deviations between the ideal situation in b and the system used in this work, d, can be seen. These deviations (clustering of particles and free space on the surface) are artifacts from the drying process, which modifies the pattern formed in suspension.

are indicated). In real systems, however, it is rarely the case that particles are immovable on the surface. This is the most common deviation from RSA models. For example, in the SEM images of Figure 2, some particles are clustered together, and as a consequence, some free space is produced on the surface. However, the particles can only move under the influence of capillary forces during drying. As long as the particles are in suspension, they will randomly adsorb, as predicted by the RSA theory, and will stick to the surface by electrostatic forces (however, many other factors might be responsible for deviations from a “pure” RSA model in this case, as mentioned later). During drying, capillary forces (stemming from water bridges that form between two particles) may be as high as the electrostatic forces holding the particles in place and therefore may move some particles together and form clusters of particles, as observed in Figure 2.

As mentioned above, two main parameters have long been identified to influence particle adsorption in cases where electrostatic interactions dominate the adsorption process: pH and ionic strength. These parameters were also tested in the silica nanoparticle–PEI system that was used in this work. It was found that particles near the isoelectric point (IEP) (at a pH of about 2.3), tend to agglomerate and form multilayers on the substrate, while with increasing pH, the particle concentration on the surface decreases because of the higher charge of the silica particles at higher pH values. Similar trends were found when lowering the ionic strength of the suspension from 160 mmol to a pure water suspension. Fewer and fewer particles

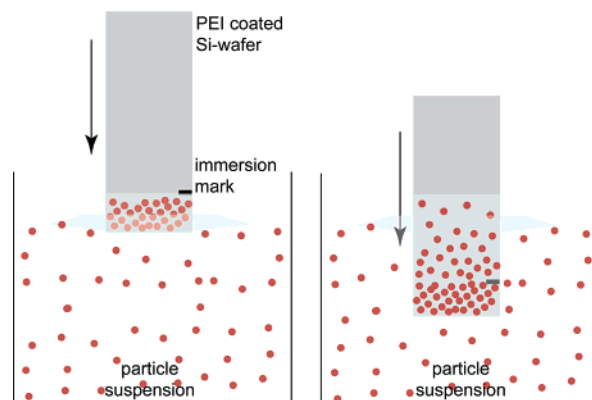


Figure 3. Schematic drawing of the situation at the commencement of the dip-coating process. The sample is immersed a few millimeters into the suspension to avoid unfavorable edge effects and to provide an area where a dense RSA monolayer can form. The immersion mark placed on the sample indicates the line from which on the actual dip-coating process starts.

adsorb to the positively charged surface because the electric double layer becomes decreasingly shielding as fewer ions are present in the suspension. This “shielding” effect of the double layer is often expressed by the Debye length, a parameter describing the “thickness” of the electric double layer. In our system, the Debye length is below 1 nm for a 160 mmol HEPES (pH 7.4 buffer) salt suspension (NaCl) and around 30 nm for a “pure water” suspension (we assume a minimum salt concentration of around 100 μ mol for practical reasons (ions from stock solution, contamination from the air and handling, etc.))

Colloidal gradients were prepared by successively exposing a surface to a colloidal suspension with known properties for a specific time interval. If the surface and the particles interact electrostatically, particles will start to adsorb and form an incomplete particle layer, the number adsorbed depending on the time for which the particles were allowed to adsorb. This process is sketched in Figure 2, which (a) shows the situation after short adsorption times and (b) represents the jamming limit of the monolayer (which is reached after a longer time interval, depending on particle concentration).

The challenge to form a colloidal topographical gradient on a substrate can therefore be tackled by exposing different parts of the substrate for increasing times to a colloidal suspension. This is most conveniently done by simply dip-coating the substrate into the colloidal suspension at a distinct speed profile. By doing so, the end of the substrate that is immersed initially remains in the suspension much longer than the end of the substrate that is only immersed during the last part of the dipping process. Removing a sample from the suspension leads to the formation of a drying front, which both disturbs the colloidal structure itself and, more importantly, causes additional colloidal particles to be dragged to the three-phase contact line. In this case, particles are not only adsorbed by electrostatic interactions but also by capillary forces, an undesired and less controllable process. Therefore, the substrate sample has to be immersed into the nanocolloid suspension. In our experiments, the substrate was immersed about 5 mm into the suspension and was held there for 30 min. Only then was the sample immersed into the suspension at a given speed profile. Figure 3 shows a schematic of the situation prior to the start of the dip-coating process on the left and the situation at the end of the dip-coating process on the right. This procedure has two advantages: first, it minimizes the influence of edge effects that occur when a sample is immersed into the suspension. For example, a “jump” occurs when the sample first touches the suspension surface and contacts the

substrate: the water film wets the sample very rapidly to form the water meniscus as depicted schematically in Figure 3. If the sample were not immersed a few millimeters into the suspension prior to the start of the experiment, such edge effects may affect the formation of the particle gradient. Second, the area where the sample was initially immersed provides a useful reference region to subsequently determine the jamming limit of the particle suspension, since this area is maintained for a significant length of time in the suspension, and thus a RSA monolayer of particles was allowed to form.

Another critical point is the end of the dip-coating process. To avoid drying effects as much as possible, the sample was not removed through the suspension–air interface. At the end of the dip-coating process, when the sample is immersed completely into the suspension (right-hand side of Figure 3), the beaker with the suspension is carefully flushed with extensive amounts of water. The beaker overflows and the suspension is rapidly diluted. After the suspension is diluted so much that ideally no more particles are present, the sample is removed from the suspension, is rinsed with more water, and is dried under a nitrogen flow. By means of this process, the influence of capillary forces during the drying process can be minimized and only a few particles are allowed to adsorb during the drying step.

Capillary forces are of great importance in such systems and are comparable in magnitude with the attractive electrostatic interactions between particle and surface. The drying step must therefore be controlled as described above. It is not an easy task to assign numbers to the capillary and electrostatic interaction energies because of assumptions that are made in the existing models, which are not always fulfilled in real systems. Nevertheless, the attractive capillary interaction energy between two particles was calculated to be about 4.4×10^6 kT for our system (on the basis of equations derived from refs 22–24). The electrostatic interaction energy between the surface (assuming a ζ -potential of 100 mV) and a particle (ζ -potential of -65 mV, as measured) is around 10^2 kT (upon contact of the two, rapidly decaying if the separation distance is increased).²⁵ This demonstrates that capillary forces are very strong compared to the electrostatic interaction energies. In fact, judging from the calculated values, they are several orders of magnitude higher than the electrostatic attraction of the particles to the surface. This is especially true if the particles are only separated by small distances. Capillary forces therefore gain in importance at high colloid densities on the surface, while they are relatively insignificant at low particle concentrations on the surface. These numbers also rationalize why very often in these experiments, doublets, triplets, or small clusters of particles are to be found on the surface instead of well-separated particles. As soon as two, three, or more particles are electrostatically adsorbed at relatively small separations, it is almost inevitable that these particles cluster together, since the capillary forces in these situations significantly exceed the electrostatic interactions.

Figure 4 shows an example of a colloidal gradient produced with 73 nm silica particles at a concentration of 0.002 wt % in pure water. An almost perfectly linear increase in particle concentration along the 1 cm gradient can be observed. Only a very few particles were adsorbed at one end, while almost a complete RSA-monolayer was formed on the other end. While there is virtually no visible influence of capillary forces on the low particle concentration images, clustering of particles increases

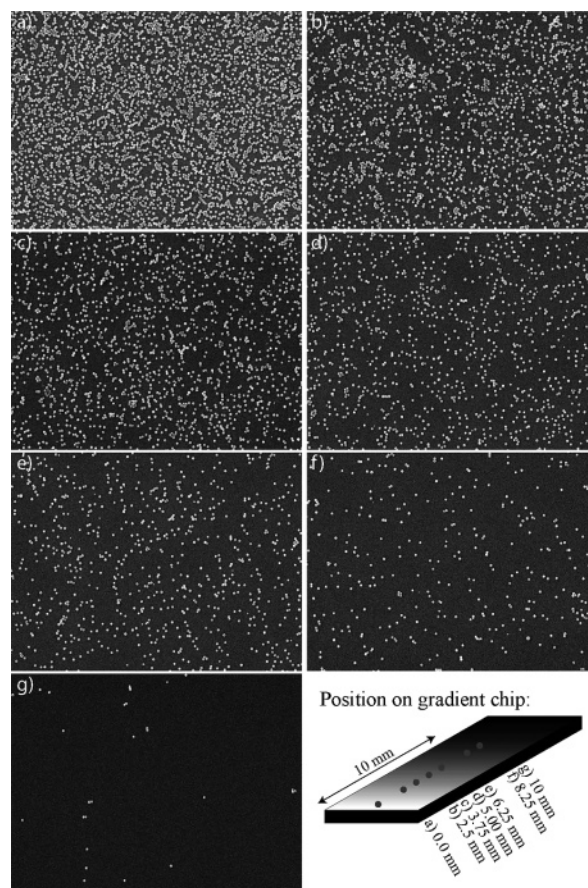


Figure 4. SEM images of a colloidal gradient and a sketch of the position of these images on the 1 cm gradient. Particle diameter was 73 nm and a particle concentration of 0.002 wt % was used in a pure water suspension. The suspension was slightly stirred during the dip-coating process, which lasted for 30 min with a designed immersion profile. The immersion profile was set to $x(t) = a(t - u)^2$, where $x(t)$ is the position on the gradient at time t , which was running from 0 to 1800 s, $u = -100$ s (a parameter needed only for technical reasons), and $a = -3 \times 10^{-6}$ m/s².

as the concentration of particles on the surface increases. This behavior is consistent with the force estimations made above, since as soon as the interparticle distance decreases, capillary forces gain in importance and tend to influence the resulting pattern more strongly. The immersion profile used (see figure caption in Figure 4) has a second-order polynomial shape to account for the \sqrt{t} dependence of the diffusion-controlled particle adsorption kinetics observed in Figure 1. The combination of a second-order polynomial immersion profile and the \sqrt{t} dependence of the particle adsorption kinetics would be expected to lead to a linear particle gradient. Stirring of the suspension during the process has a distinct influence on the particle gradient formation (causing far more particles to adsorb, in comparison to static conditions). Without stirring, particle coverage on the surface reached no more than 5%, while in the case of the gradient experiments, more than 30% coverage was obtained.

In the real system, this linearization of the particle gradient proved to work rather successfully, as observed in Figure 5. Here, SEM images were analyzed and statistical examination of these images yielded the particle concentration as a function of the position on the gradient (see Figure 5). It is observed that the particle gradients evolve nearly linearly over the entire 1 cm gradient. The gradient can be expanded to 2 cm by simply adapting the parameters such that instead of 10 mm, 20 mm will be dip-coated during the 1800 s. The value for the highest particle

(22) Aizenberg, J.; Braun, P. V.; Wiltzius, P. *Phys. Rev. Lett.* **2000**, *84*, 2997.

(23) Kralchevsky, P. A.; Nagayama, K. *Langmuir* **1994**, *10*, 23.

(24) Paunov, V. N.; Kralchevsky, P. A.; Denkov, N. D.; Nagayama, K. J. *Colloid Interface Sci.* **1993**, *157*, 100.

(25) Ninham, B. W. *Adv. Colloid Interface Sci.* **1999**, *83*, 1.

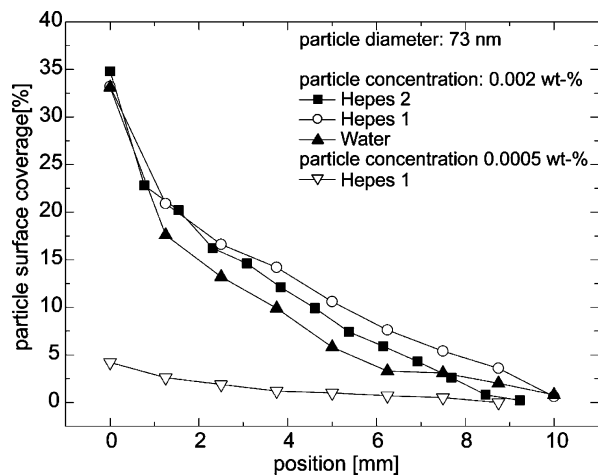


Figure 5. Colloid coverage of selected 1 cm gradients as a function of position on the gradient. Statistical evaluation of SEM images from different positions on the colloidal gradients yields the colloid coverage over the whole gradient. Particle suspensions with 0.002 wt % silica particles (73 nm in diameter) were used in different solvents. There is no significant difference between HEPES 1 and 2 buffered suspensions and ultrapure water suspensions (which were at pH 9.9). The end coverage reached values between 32 and 37%. The end coverage was measured in the area below the “immersion mark” indicated in Figure 3. This explains why this first point (at position 0 cm) is slightly higher than expected from the other values on the gradient, which lie on a rather straight line. If particle concentration was 4 times lower than for the first three experiments, the end coverage was significantly lower (around 5%), but the gradient still shows very linear behavior but in a narrower coverage range.

coverage (at position 0 cm) is taken within the area below the “immersion mark” (see Figure 3) and is therefore a little higher than one would expect from the extrapolation of the other values. This first value can be considered to be the particle coverage near the jamming limit and was found in this work to be in the range of 32–37%. This value is considerably lower than the theoretical value of 54.7% found in RSA-models. However, it must be remembered that in this theoretical model, no electric double layer is taken into account, which must be added to the particle diameter. It must also be stressed that the adsorption process of such small particles is influenced by many other factors, such as Brownian motion, the exact nature of the polymeric adlayer (bridging effects, mobility of particles on a polymeric adlayer), surface charge distribution, and others, and thus, it is not possible to attribute the adsorption process to a simple RSA-model. Also, capillary forces disturb the pattern formation to some extent near the jamming limit, such that statistical analysis underestimates the true particle coverage.

Another convenient way of changing the morphology of the produced particle gradients besides simply changing the particle size is to expose the colloidal gradient to a heat-treatment procedure. This will have two effects on the particle gradients. For one, all organic components used during the production of the gradient will be burned off, and second, the colloidal particles will start to sinter onto the substrate. The sintering process will thus increase mechanical stability of these gradients considerably, and by controlling the sintering conditions, the morphology of the particles may be changed in a predictable way. Figure 6 shows the influence of such a sintering treatment on the evolution of the particle morphology. During the heat-treatment step, the temperature was always maintained at the chosen sintering temperature for 2 h. Surface diffusion in the silica nanoparticles was activated at temperatures around 1100 °C. Below 1075 °C, there was no evidence of sintering and the particles remained in

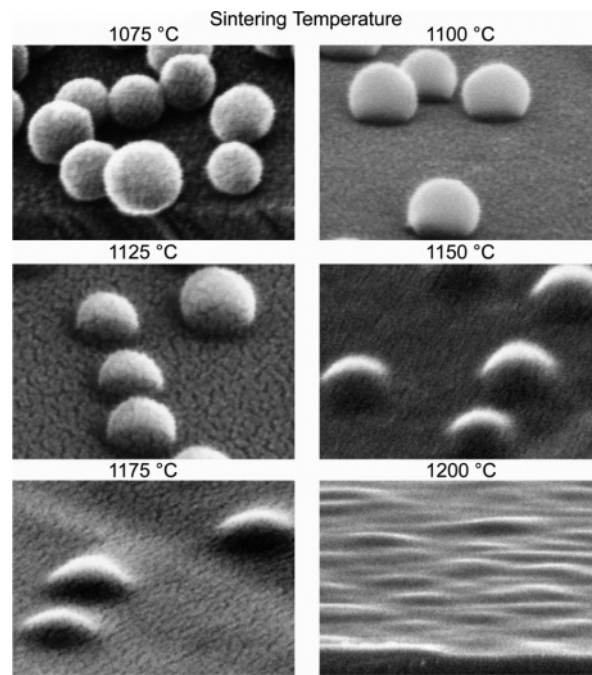


Figure 6. SEM images of heat-treated colloidal silica particles (73 nm in diameter) (tilted view). Heat treatment consisted of heating the samples to the desired temperature (with about 10 °C/min), holding at the end temperature for 2 h, and passive cooling (which took several hours). In the interesting temperature regime (1075–1200 °C), particle morphology changes continuously with increasing sintering temperature, as observed in the images. Below 1075 °C, the temperature is not high enough to induce surface diffusion on the silica particles and no change in particle morphology was seen. Temperatures above 1200 °C are sufficient to sinter the particles completely together with the oxidized silicon wafer surface, while at 1200 °C traces of the particles are still seen.

a spherical shape on the surface. With increasing temperature, the particles began to sinter to the surface. At 1100 and 1125 °C, the effects are not as dominant, but a slight “neck formation” was already evident. This neck formation is typical for the onset of the sintering process and is associated with the diffusion of surface atoms from the colloidal particle to the contact region of the particle with the substrate. The surface diffusion of atoms alone will not lead to shrinkage of the particles as observed for temperatures higher than 1150 °C. At these temperatures, other diffusion mechanisms are also active, such as volume diffusion (matter is transported from the bulk of the particle to the neck region) and diffusion along the particle–substrate interface. Both of these diffusion-transport mechanisms are responsible for the shrinkage of the particles at higher temperatures. The driving force for these sintering/diffusion processes is related to the minimization of the free surface energy that can be achieved as the spherical particles gradually minimize their surface area. The end point of this process is reached for temperatures above 1200 °C, where the particles lose their shape and completely diffuse into the surface. Figure 6 illustrates these steps and depending on the sintering conditions, the morphology of the particle gradient can be tailored. In Figure 7, the apparent contact angle of the particle with respect to the surface as determined from SEM image analysis is plotted versus the sintering temperature. A linear relation between the two is found, which allows the precise tuning of the morphology of our particle gradients. Corresponding to this change in contact angle, a change in the height of the colloidal particles is observed. The particle height changes in a similar way as the contact angle. At low temperatures, the particle height is equal to the particle diameter

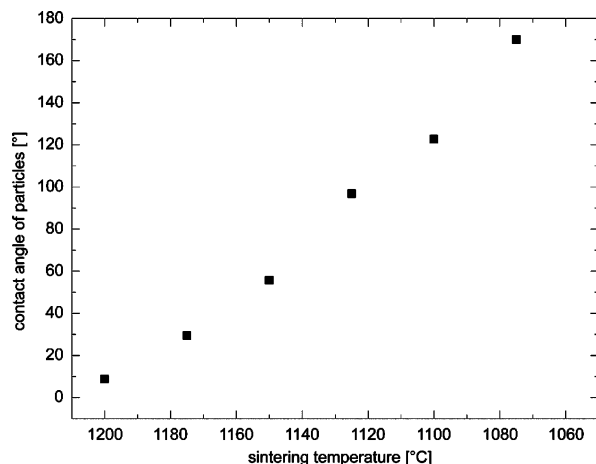


Figure 7. Graph of apparent contact angle of particle on a colloidal gradient versus sintering temperature. A linear relation between the contact angle (determined from SEM images as presented in Figure 6) and the sintering temperature is observed. Sintering at higher temperatures allows the spherical silica particles to diffuse much better into the surface and the spherical particles can decrease their large surface area more efficiently. This surface area reduction upon sintering is the driving force for the sintering process and as soon as surface diffusion processes are activated, the particle morphology starts to change. At lower sintering temperatures, fewer diffusion processes are activated and consequently only little influence on the particle morphology is observed.

and decreases with increasing sintering time. At high temperatures (above 1200 °C), the particle height decreases to 0 and the topography pattern vanishes. Thus, the heat treatment is an effective way of changing the particle topography on the gradient from large, spherical particles to small “hill-like” structures at higher temperatures.

Beside the adjustability of the morphology of the particle gradients that is offered by this sintering process, the mechanical stability is increased drastically: the particles are no longer simply adsorbed but are firmly sintered onto the surface. This fact makes these gradients also useful for several applications for which particle arrays were not previously suited, for example in adhesion and friction studies or as templates in replication techniques.²⁶ Choosing sintering conditions such that the contact angle of the particles is below 90° (particles appear as half-spheres on the sample) allows such samples to be used as templates since no “undercutting” during a replication process (casting in PDMS, for example) would be observed.

A first example of how such particle gradients can be useful is shown in Figure 8. Fluorescent labeling of the actin filaments and the nuclei of these cells is shown in the top two fluorescence microscopy images. It is observed that cell adhesion and spreading is largely reduced in areas where the density of particles on the surface is high (left side of fluorescence images). With decreasing particle density, the number of cells growing on the substrate increases significantly and reaches the highest number in the areas where no particles were on the surface (on the right-hand side of the fluorescence images). The graph in Figure 8 quantifies these results and indeed an inverse dependence of cell number with particle density is found. These are initial, promising results from cell biology experiments carried out with this kind of colloidal gradients and more detailed studies are currently underway.²⁷ This experiment is a good example of how such

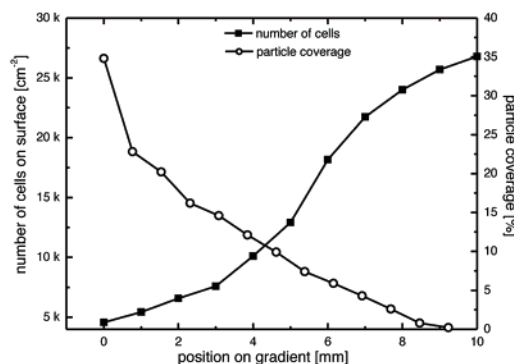
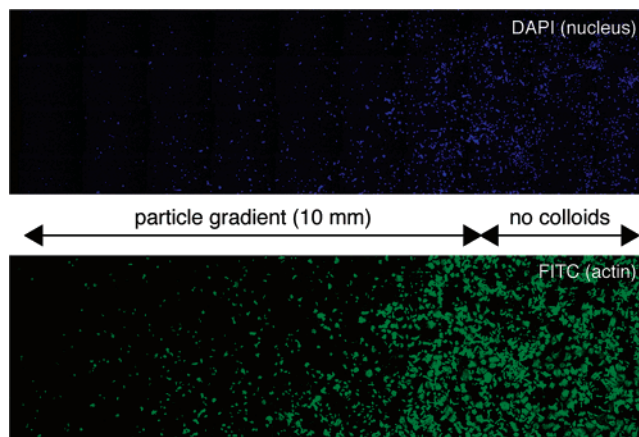


Figure 8. Fluorescence microscopy images of stained actin filaments (FITC) and cell nuclei (DAPI) on a particle gradient (0.002 wt % in H₂O). The particle gradient was uniformly coated with PLL-g-PEG-RGD, a polymer that introduces the RGD function, a peptide sequence known to induce cell growth, onto the particle surface. At high particle surface coverage (to the left of the images), only a few cells adhere and spread on the surface, while with decreasing particle density (moving to the right-hand side of the fluorescence microscopy images) the number of cells increases significantly. Quantitative analysis (graph below the images) shows how indeed a reciprocal relation exists between particle surface coverage and the number of rat calvarial osteoblast cells growing on the substrate.

nanomorphology gradient surfaces will help in rapid screening tests and how combinatorial and diagnostic studies can be performed on a single sample in the future. The techniques presented here may help in fabricating suitable particle gradients for these kind of applications in a straightforward and customizable way.

Conclusion

Combining the knowledge gained from particle-adsorption experiments as a function of particle concentration, pH, and ionic strength with a dip-coating process led to the development of a colloidal patterning method that allows the production of colloidal gradients with specifically adjustable parameters on a centimeter-length scale. Because of the nature of this process, almost any material combination could be used in a similar way to produce a similar kind of particle gradient provided that the adsorption kinetics are known and can be controlled as shown here. In this work, silica nanoparticles were assembled into a gradient on a silicon wafer, but no significant difference would be expected if the substrate material were changed to a different metal oxide, provided that appropriate modifications are made to account for differences in IEPs, adsorption kinetics, and sintering temperatures.

(26) Wieland, M.; Chehroudi, B.; Textor, M.; Brunette, D. M. *J. Biomed. Mater. Res.* **2002**, *60*, 434.

(27) Kunzler, T. P. Diss. ETH No. 17049, ETH Zurich, Zurich, 2007.

The subsequent sintering process proved to be an efficient way of altering the morphology of the colloidal gradients. The globular shape of the adsorbed particles can be continuously changed as a function of the exact sintering conditions. Furthermore, this heat treatment provides a route to stabilize the colloidal array on the surface. Thus, mechanically stable, topographical gradients were produced using a versatile technique that may find applications in various fields because of their tunable properties.

Acknowledgment. The authors thank Michael Horisberger for the metal oxide coatings (PSI, Switzerland) and Brandon Bürgler for SEM imaging (ETH Zürich). This work was financially supported by the ETH Council Nanotechnology funding program, Top Nano 21 (Project 5971.2), as well as by Nanocues (EU: FP6-NMP) and ETH Zurich.

LA0700422